Macromolecules

pubs.acs.org/Macromolecules Article

Ultra-Fast, One-Pot Synthesis of Nanofibers by Lewis Pair Polymerization-Induced Self-Assembly

Chengkai Li,[#] Wuchao Zhao,[#] Jianghua He,* and Yuetao Zhang*

Cite This: *Macromolecules* 2024, 57, 7013−7019 Read Online

ABSTRACT: Owing to their wide application potentials resulting from high aspect ratio, morphologically pure nanofibers attract intense attention but remain challenging to synthesize due to their narrow synthetic experimental window. Here, we employed strong nucleophilic *N*-heterocyclic olefin (NHO) as a Lewis base (LB) and a bulky organoaluminum compound as a Lewis acid (LA) to construct a Lewis pair (LP), which can rapidly prepare a series of diblock copolymers (di-BCPs), poly(trifluoroethyl methacrylate)-*b*-poly(heptadecafluorodecyl methacrylate) (PTFEMA-*b*-PHDFDMA), through the sequential monomer addition method. The liquid-crystalline characteristics of PHDFDMA, in combination with Lewis pair polymerization-induced self-assembly (LP-PISA) strategy, enable ultrafast, one-pot synthesis of di-BCPs with fiber morphologies (dimeters = 11.7−25.1 nm) across a wide experimental window and solid contents (up to 20% w/w). These di-BCPs are structurally characterized by ^{1}H nuclear magnetic resonance spectroscopy, differential scanning calorimetry, and small-angle X-ray scattering and morphologically analyzed by transmission electron microscopy. This LP-PISA strategy provides the possibility of achieving the desired morphology with well-defined structure and purity through precise control over the evolution parameters.

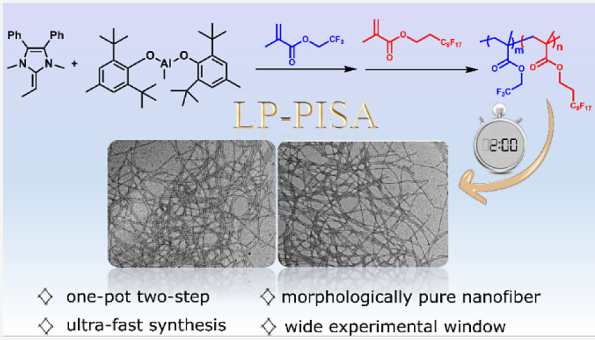

■ INTRODUCTION

Being a powerful tool for synthesis of nanomaterials, self-assembled amphiphilic AB-typed diblock copolymers (di-BCPs) have received intense attention due to their wide application potentials in biomedicine, additives, nanoreactors, and more.[1−6] Solution self-assembly is typically employed to synthesize nanoparticles by postpolymerization in highly dilute solutions, thereby greatly restricting its practical application.[7,8] Polymerization-induced self-assembly (PISA) was developed to simultaneously achieve both the amphiphilic copolymers and self-assemblies at high solid contents (up to 50 wt %).[9−12] Significant progress has been made in the application of various living polymerization techniques to PISA.[13−20] A full range of morphologies (spheres, fibers/worms, vesicles, and lamellae) could be obtained through PISA by adjusting the length of solvophilic and solvophobic blocks, solid contents, and solvents.[21−27] Among these, fiber morphology is of particular interest due to their large surface area and anisotropic structure.[28−32] This makes them highly applicable in various fields such as drug delivery, Pickering emulsions, super flocculants, organic photovoltaic devices, and molecular separations.[33−37] Crystallization-driven self-assembly (CDSA) is a powerful method for synthesizing fiber morphologies through the crystallization of hydrophobic blocks with controlled lengths. However, this method typically requires highly dilute concentrations and multistep synthetic procedures.[7,31,38−41] Introducing supramolecular structures to the polymer chains or using liquid-crystalline (LC) polymers as hydrophobic blocks can enable the synthesis of fiber morphologies under high concentrations, but these approaches require purification processes and long reaction times, thus impairing the synthetic efficiency of PISA.[29,37] Moreover, the experimental windows for synthesis of fibers are typically narrow, so it remains a great challenge to synthesize morphologically pure nanofibers with varying lengths and diameters.[42,43] Therefore, it is highly desirable to develop a simple and efficient PISA strategy for fiber morphology synthesis.

Being a newly emerged and powerful polymerization strategy, Lewis pair polymerization (LPP) has accomplished many excellent examples in polymer synthesis. These include living polymerization of various types of monomers, chemo- and regioselective polymerization of divinyl monomers, precise synthesis of polymers with controlled molecular weight (up to 2197 kg/mol), flexible regulation of the monomer sequence (up to 63-block numbers) and different topologies (linear, star,

Received: April 5, 2024
Revised: July 3, 2024
Accepted: July 5, 2024
Published: July 19, 2024

Scheme 1. (a) Structures of Lewis Acids and Lewis Bases. (b) Synthesis of Amphiphilic PTFEMA-*b*-PHDFDMA di-BCPs by LP-PISA

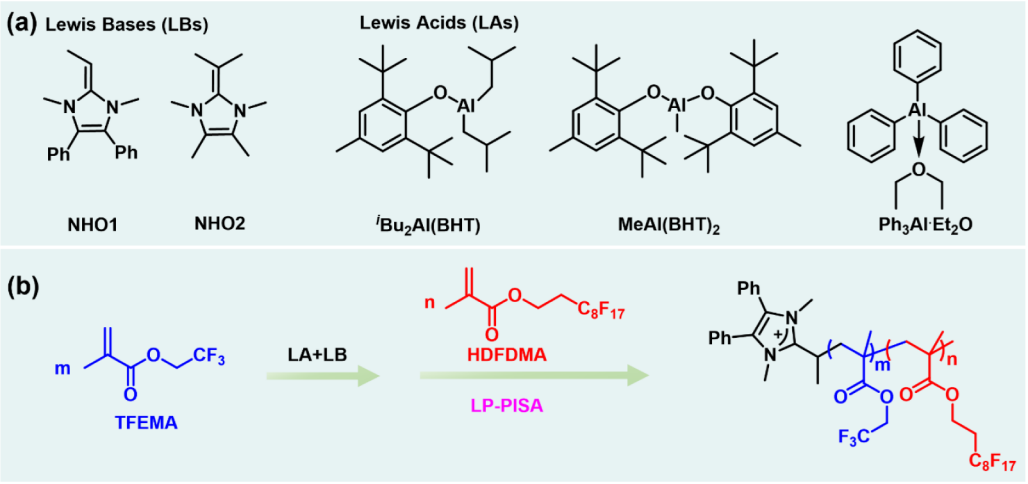

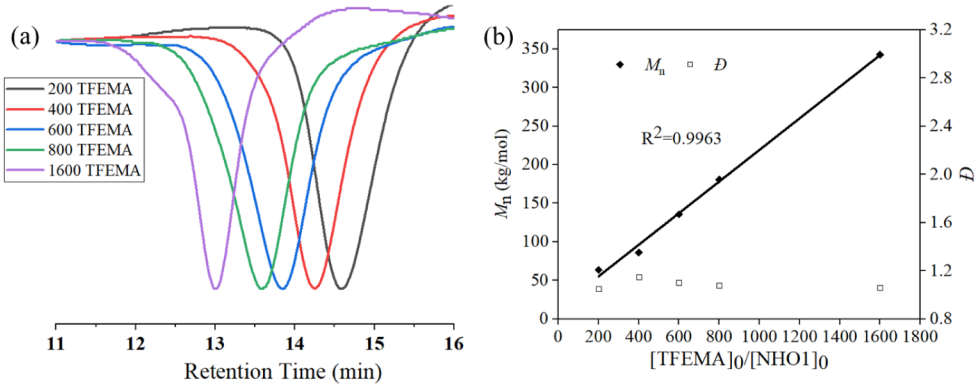

Figure 1. (a) GPC traces of PTFEMA samples prepared from polymerization performed at various $[TFEMA]_0/[NHO1]_0$ ratios at RT. Conditions: $[TFEMA]_0/[NHO1]_0/[MeAl(BHT)_2]_0$ = 200:1:2, 400:1:2, 600:1:2, 800:1:2, and 1600:1:2 and $[TFEMA]_0$ = 1 M. The negative GPC signal is due to the lower refractive index of fluoropolymer than that of the eluent. (b) Plots of M_n and $Đ$ for the PTFEMA vs $[TFEMA]_0/[NHO1]_0$ ratio.

and cyclic).[44−58] Recently, we employed LPP to obtain di-BCPs with different morphologies, which prompted us to address the above-described issues related to fiber synthesis through LP-PISA.[59] Thanks to the LC characteristics of poly(heptadecafluorodecyl methacrylate) (PHDFDMA) and excellent control of LPP, we successfully prepared amphiphilic PTFEMA-*b*-PHDFDMA di-BCPs with nanofiber morphology over a broad experimental window through an ultrafast, one-pot, two-step process. The diameters of the fibers can be tailored in the range of 11.7−25.1 nm, simply by adjusting the molar mass of the blocks and solid contents. The LC ordering of PHDFDMA was also characterized by differential scanning calorimetry (DSC) and small-angle X-ray scattering (SAXS).

■ RESULTS AND DISCUSSION

TFEMA Homopolymerization. Fluorinated polymers exhibit superior properties compared to that of the unfluorinated ones, including high hydrophobicity, excellent chemical and thermal properties, tunable lipophilicity, low refractive index, and low surface energy.[60,61] PISA relies on the chain extension of a living block soluble in a selective solvent with a second monomer to generate a nonsoluble block. Due to the poor solubility of fluorinated polymers in common organic solvents, it can serve as the second monomer to generate a nonsoluble block, thereby expanding the monomer library of PISA. Additionally, in order to synthesize amphiphilic block copolymers via PISA, it is a requisite to first obtain a soluble living block. Therefore, semifluorinated methacrylates, trifluoroethyl methacrylate (TFEMA), and heptadecafluorodecyl methacrylate (HDFDMA) were selected for PISA to maintain the balance between the solubility of monomers and polymers in solvents. First, two strong nucleophilic *N*-heterocyclic olefins (NHOs) (NHO1 and NHO2) and three organoaluminum compounds with different steric hindrance and Lewis acidity (Scheme 1a) were employed as Lewis bases (LBs) and Lewis acids (LAs) for the polymerization of TFEMA, respectively, due to their demonstrated excellent activity in (meth)acrylate polymerization.[55,59,62] Control experiments indicated that NHO1 obtained only 4% conversion of 200 equiv of TFEMA in fluorobenzene (FB) in up to 24 h, whereas NHO2 can convert 77% of monomers to polymer within 150 min (runs 1 and 2, Table S1). The effectiveness of LAs was also examined for the polymerization of TFEMA. 21% monomer conversion was obtained by $^iBu_2Al(BHT)$ alone and 7% conversion was obtained by $Ph_3Al{\cdot}Et_2O$, whereas $MeAl(BHT)_2$ showed no activity for the polymerization of TFEMA in 24 h (runs 3−5, Table S1). To avoid the background polymerization initiated by LB or LA itself, NHO1 and $MeAl(BHT)_2$ were selected and a Lewis pair was constructed to examine the polymerization of

https://doi.org/10.1021/acs.macromol.4c00768
Macromolecules 2024, 57, 7013−7019

Table 1. PISA Results[a]

run	LB/LA/TFEMA/HDFDMA	solid content (%)	time (min)	conv.[b] (%)	morphology[c]	diameter (nm)[c]
1	1/2/100/25	15	1/1	100/100	fiber	11.2
2	1/2/100/40	15	2/3	100/100	fiber	13.8
3	1/2/100/25	20	1/1	100/100	fiber	11.7
4	1/2/100/40	20	1/2	100/100	fiber	21.8
5	1/2/100/25	5	5/5	100/100	fiber	13.7
6	1/2/100/50	5	5/6	100/100	fiber	22.5
7	1/2/200/25	15	3/4	100/100	fiber	13
8	1/2/200/50	15	3/4	100/100	fiber	16.5
9	1/2/200/75	15	3/7	100/100	fiber	18.3
10	1/2/200/25	5	7/3	100/100	fiber	15.2
11	1/2/200/50	5	14/26	100/100	fiber	17.1
12	1/2/200/75	5	20/20	100/94	fiber	20.9
13	1/2/200/75	10	6/9	100/100	fiber	15.8
14	1/2/200/50	20	6/9	100/100	fiber	14.5
15	1/2/200/75	20	2/5	100/100	fiber	18.4
16	1/2/300/50	15	5/4	100/100	fusiform+short fiber	14.5
17	1/2/300/75	15	6/3	100/79	fusiform+short fiber	17.3
18	1/2/300/125	15	7/18	99/100	fusiform+short fiber	28.5
19	1/2/300/100	10	10/20	100/100	fusiform	62.2/24.5[d]
20	1/2/300/75	20	4/3	100/100	long fiber+short fiber+fusiform	18.1
21	1/2/600/100	15	20/55	100/100	fusiform	60.7/25.5[d]
22	1/2/600/200	15	35/43	100/80	fusiform	71.9/39.2[d]

[a]Condition: carried out at ambient temperature (~25 °C) in FB at solid contents of 5−20 wt %, where solid content = [m (catalysts) + m (monomers)]/[m (catalysts) + m (monomers) + m (solvent)] × 100%. [b]Monomer conversion was measured by ^{1}H NMR spectroscopy. [c]Morphologies were determined by TEM. [d]The length and width of the fusiform.

TFEMA. Quantitative monomer conversion was obtained in 1 min for the polymerization performed in a 200:1:2 $[TFEMA]_0/[NHO1]_0/[MeAl(BHT)_2]_0$ ratio (run 6, Table S1), furnishing PTFEMA with M_n = 63.5 kg/mol and $Đ$ = 1.05. Increasing the $[TFEMA]_0/[NHO1]_0$ ratio from 200 to 1600, full monomer consumptions can be obtained for all of the investigated ratios, producing polymers with predicted M_n and narrow $Đ$ (runs 6−10, Table S1). GPC traces showed a gradual shift to higher molar mass regions, while maintaining narrow and unimodal distribution (Figure 1a). The M_n values of the resulting PTFEMA increased linearly (R^2 = 0.996) from 63.5 to 343 kg/mol as the monomer-to-LP ratio increased from 200 to 1600, while the $Đ$ values were kept in a narrow range between 1.05 and 1.15 (Figure 1b). Furthermore, a plot of PTFEMA M_n vs monomer conversion at a fixed $[TFEMA]_0/[NHO1]_0/[MeAl(BHT)_2]_0$ ratio of 400:1:2 also gave a straight line (R^2 = 0.996), which was coupled with the small $Đ$ values (Figure S2). The analysis of the low-MW PTFEMA sample with matrix-assisted laser desorption/ionization time-of-flight mass spectroscopy (MALDI-TOF MS) revealed that the polymer produced by NHO1/$MeAl(BHT)_2$ is a linear polymer chain capped with NHO1/H groups (Figures S3 and S4). In contrast, a few series of molecular ion peaks were detected for the PTFEMA produced by NHO alone, where the major series corresponds to linear PTFEMA capped with NHO2 and cyclic β-ketoester or δ-valerolactone chain ends resulting from backbiting side reactions (Figures S5 and S6), indicating that the polymerization by NHO2 alone is not living and controlled.

Our previous work revealed that the reaction of NHO1 and $MeAl(BHT)_2$ formed a pure classic Lewis adduct (CLA).[55] While the stoichiometric reaction performed in a 1:1:1 NHO1:$MeAl(BHT)_2$:TFEMA ratio produced zwitterionic enolaluminate intermediates as two isomers (Figure S7), this polymerization adopted a bimolecular activation mechanism. In order to verify the livingness feature of this polymerization, chain extension experiments were performed by adding the second batch of monomers after completion of the first batch of monomers without quenching. GPC traces of the resulting polymers shifted to the higher-molar-mass region and showed a narrow and unimodal molecular weight distribution (MWD) (Figure S1). The third batch of monomers can still be fully consumed. The M_n values of the polymers produced from the chain-extension experiments increased from 63.5 to 88.5 to 114 kg/mol, respectively (runs 1−3, Table S2). All of these results clearly demonstrated the excellent controllability of NHO1/$MeAl(BHT)_2$ LP over the TFEMA polymerization. Therefore, NHO1/$MeAl(BHT)_2$ was selected for the following investigations.

Dispersion Polymerization of HDFDMA. After obtaining this soluble, living PTFEMA polymer chain, we turned our focus to its application in PISA. Due to the LC characteristics and insolubility of PHDFDMA in FB, HDFDMA was utilized as core-forming monomer to copolymerize with TFEMA through a sequential monomer addition method, with 5−20% solid contents (Scheme 1b). First, with a fixed degree of polymerization (DP) of PTFEMA at 100 and solid content at 15%, after completing TFEMA within 1 min, HDFDMA was added at DP = 25, and full monomer conversion was obtained within 1 min as revealed by ^{1}H NMR spectroscopy (run 1, Table 1). Due to their poor solubility in common organic solvents, the resulting copolymers were not analyzed by GPC. By using 1,3-bis(trifluoromethyl)benzene as a cosolvent (1,3-bis(trifluoromethyl)benzene:$CDCl_3$ = 1:5 v/v), the copolymers were characterized by ^{1}H NMR spectroscopy, which confirmed that the composition of the produced copolymers is consistent with that of the target $PTFEMA_{100}$-*b*-$PHDFDMA_{25}$ di-BCPs (the subscripts represent the DP of each block, Figure

https://doi.org/10.1021/acs.macromol.4c00768
Macromolecules 2024, 57, 7013−7019

S8). Moreover, transmission electron microscopy (TEM) images revealed the formation of pure nanofibers with an average diameter of 11.2 nm (Figure 2a). With the DP of PHDFDMA increasing to 40, pure nanofibers could still be obtained within 5 min and the average diameters of nanofibers increased to 13.8 nm (Figure 2b). To the best of our knowledge, it is the first time that pure nanofibers have been prepared in such a short time using the PISA strategy.[63,64]

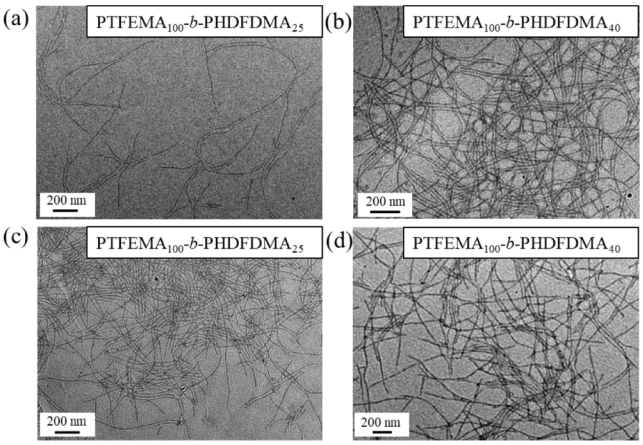

Figure 2. TEM images for various di-BCP nanoparticles prepared by LP-PISA: (a) PTFEMA$_{100}$-*b*-PHDFDMA$_{25}$ at 15 wt % solid content; (b) PTFEMA$_{100}$-*b*-PHDFDMA$_{40}$ at 15 wt % solid content; (c) PTFEMA$_{100}$-*b*-PHDFDMA$_{25}$ at 20 wt % solid content; (d) PTFEMA$_{100}$-*b*-PHDFDMA$_{40}$ at 20 wt % solid content.

Solid content is also found to play an essential role in affecting the morphologies of the assemblies. Therefore, we further investigated the effects of solid content on morphologies and found that with the solid contents ranging between 5% and 20%, pure nanofibers were obtained as the only morphology, with average diameters in the range of 11.7−22.5 nm (runs 3−6, Table 1, Figures 2c,d and S13,14). To examine the capability of LP-PISA in synthesizing a pure nanofiber phase with a wider experimental window, we fixed the solvophilic PTFEMA at DP = 200 and varied the DP of PHDFDMA from 25 to 50, and 75, respectively. For the copolymerization performed with PHDFDMA at DP = 25, short nanofibers were obtained with an average diameter = 13 nm in 7 min (run 7, Table 1, and Figure S15), while the average diameter increased to 16.5 and 18.3 nm, as the DP of PHDFDMA increased to 50 and 75, respectively (runs 8 and 9, Table 1, and Figure S16). TEM images showed that the nanofibers could be produced by the polymerization performed with solid contents ranging between 5% and 20% (runs 10−15, Table 1, Figures S17−22). These results obtained at different DPs and solid contents showed that the experimental window for the synthesis of pure nanofibers is very wide, highlighting the robustness of this LP-PISA strategy.

As the LC ordering is the important driving force for the formation of nanofibers in a large experimental window, SAXS was employed to identify the phase structures of a series of di-BCP samples. Both PTFEMA$_{200}$-*b*-PHDFDMA$_{25}$ and PTFEMA$_{200}$-*b*-PHDFDMA$_{50}$ exhibited a principle scattering peak q = 1.99 nm^{-1}and a second order peak at q = 3.99 nm^{-1}, where the position of the second order peak was two times that of the principle scattering peak (Figure 3a). It is also noted that the interlayer spacing of lamellae calculated from the position of the principal scattering peak, q (as $d = 2\pi/q$), is 3.16 nm, which is almost twice the length of the extend side-chain length of PHDFDMA (1.59 nm) (Figure S26). In combination with the fact that there is no observation of scattering peak in the SAXS spectrum of PTFEMA, the LC phase of the PHDFDMA in the assemblies should be the smectic A (SmA) phase. Moreover, DSC was utilized to determine the SmA-to-isotropic phase transition temperature (T_c) of the above-described three samples (Figure 3b). It turned out that there is no T_c observed for PTFEMA homopolymer, while it is 83 °C for PTFEMA$_{200}$-*b*-PHDFDMA$_{25}$ and 88 °C for PTFEMA$_{200}$-*b*-PHDFDMA$_{50}$, which further confirmed that the stability was increased as the length of PHDFDMA increased.

Study of the Morphology Evolution. To understand the morphology evolution of the nanofibers and identify the structures of important intermediates, we further investigated the influencing effects of PTFEMA with longer length on PISA. As expected, with a fixed 300 DP of PTFEMA and 15 wt % solid content, copolymerization performed with the DP of PHDFDMA at 50 obtained PTFEMA$_{300}$-*b*-PHDFDMA$_{50}$ assemblies as a mixture of fusiform micelles and short fiber-like micelles (run 16, Table 1, Figure 4a). These short fiber-like micelles might form by fusing fusiform micelles into dimers, trimers, and longer structures. Increasing the DP of PHDFDMA from 50 to 75 or 125 resulted in mixed morphologies, with both the length and width of the fusiform micelles increasing (Figures 4b and S23, runs 17 and 18, Table 1). At a 10 wt % solid content, pure fusiform micelles were obtained for PTFEMA$_{300}$-*b*-PHDFDMA$_{100}$ assemblies (length

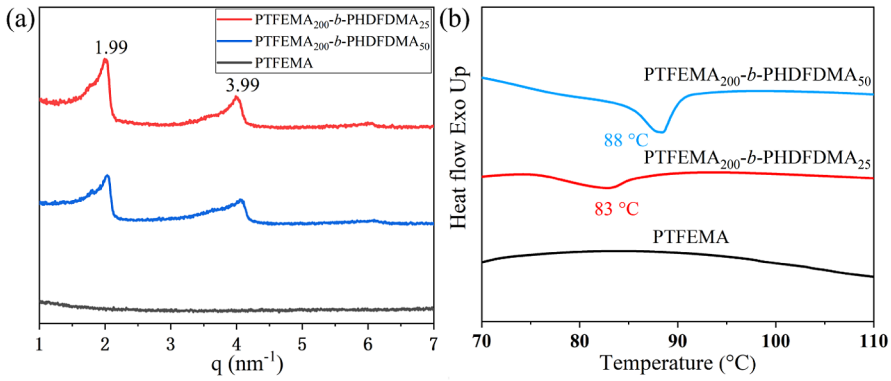

Figure 3. (a) SAXS spectra of PTFEMA, PTFEMA$_{200}$-*b*-PHDFDMA$_{25}$ and PTFEMA$_{200}$-*b*-PHDFDMA$_{50}$; (b) DSC curves of PTFEMA, PTFEMA$_{200}$-*b*-PHDFDMA$_{25}$ and PTFEMA$_{200}$-*b*-PHDFDMA$_{50}$.

https://doi.org/10.1021/acs.macromol.4c00768
Macromolecules 2024, 57, 7013−7019

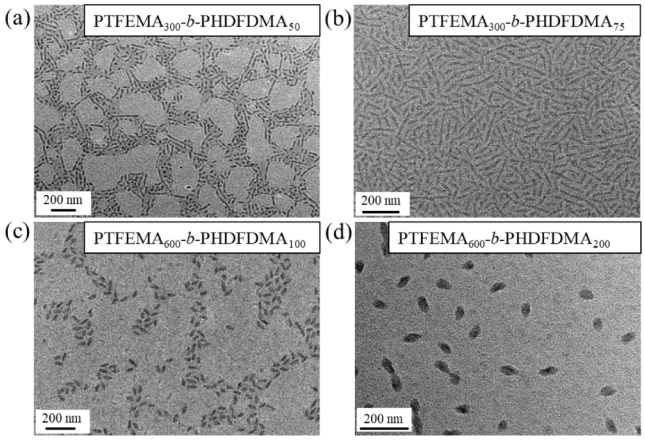

Figure 4. TEM images for various di-BCP nanoparticles prepared at 15 wt % solid contents at RT: (a) PTFEMA$_{300}$-*b*-PHDFDMA$_{50}$; (b) PTFEMA$_{300}$-*b*-PHDFDMA$_{75}$; (c) PTFEMA$_{600}$-*b*-PHDFDMA$_{100}$; (d) PTFEMA$_{600}$-*b*-PHDFDMA$_{200}$.

= 62.2 nm, width = 24.5 nm, run 19, Table 1, and Figure S24). However, at 20% solid content, PTFEMA$_{300}$-*b*-PHDFDMA$_{75}$ assemblies were obtained with mixed morphologies including long fibers, short fibers, and fusiform micelles (run 20, Table 1, and Figure S25), which is consistent with the previous results suggesting that high solid content may be beneficial for the formation of pure high-order morphologies (such as fiber/worms or vesicles).[21,42,65] With the DP of PTFEMA set at 600, only pure fusiform micelles were formed regardless of whether the DP of PHDFDMA was 100 or 200 (length = 60.7 or 71.9 nm, width = 25.5 or 39.2 nm, Figure 4c,d, runs 21 and 22, Table 1), confirming that nanofibers originate from the fusion of fusiform micelles. Thanks to the excellent controllability, high synthetic efficiency, and wide experimental window of this LP system, polymeric nanofibers with adjustable width and length can be prepared. These fluorinated nanofibers are expected to show application potentials in the additives of epoxy resins to enhance the fracture resistance, thermoresponsive materials, and ^{19}F magnetic resonance image agent.[34,66,67]

■ CONCLUSION

In summary, we have developed a highly efficient NHO-based LP to realize living/controlled polymerization of semi-fluorinated methacrylates, TFEMA. Using a sequential monomer addition method, PTFEMA-*b*-PHDFDMA di-BCPs were synthesized with a well-defined structure in a one-pot two-step process. The smectic ordering of solvophobic PHDFDMA, coupled with the LP-PISA strategy, enabled the ultrafast synthesis of nanofiber morphologies (11.7−25.1 nm) across a wide experimental window of 5−20% solid contents, achieved by changing the TFEMA to HDFDMA ratio. The well-defined LC ordering of PTFEMA-*b*-PHDFDMA di-BCPs were also confirmed by SAXS and DSC analysis. Investigations into morphology evolution indicated that the nanofibers are formed through the fusion of fusiform micelles. The LP-PISA strategy, without the requirement for isolation and purification of macroinitiators, exhibited significantly enhanced synthetic efficiency, thereby paving the way for large-scale production of assemblies in the future.

■ ASSOCIATED CONTENT

Supporting Information

The Supporting Information is available free of charge at https://pubs.acs.org/doi/10.1021/acs.macromol.4c00768.

General experimental methods, synthesis and characterization details, general polymerization methods and polymer characterization, some other polymerization results, and collected NMR (^{1}H, ^{13}C) spectra (PDF)

■ AUTHOR INFORMATION

Corresponding Authors

Jianghua He − *State Key Laboratory of Supramolecular Structure and Materials, College of Chemistry, Jilin University, Changchun, Jilin 130012, China*; Email: hjh2015@jlu.edu.cn

Yuetao Zhang − *State Key Laboratory of Supramolecular Structure and Materials, College of Chemistry, Jilin University, Changchun, Jilin 130012, China*; orcid.org/0000-0002-6406-1959; Email: ytzhang2009@jlu.edu.cn

Authors

Chengkai Li − *State Key Laboratory of Supramolecular Structure and Materials, College of Chemistry, Jilin University, Changchun, Jilin 130012, China; SINOPEC Beijing Research Institute of Chemical Industry, Beijing 100013, China*

Wuchao Zhao − *State Key Laboratory of Supramolecular Structure and Materials, College of Chemistry, Jilin University, Changchun, Jilin 130012, China*; orcid.org/0000-0002-1592-6653

Complete contact information is available at: https://pubs.acs.org/10.1021/acs.macromol.4c00768

Author Contributions

#C.L. and W.Z. contributed equally to this work.

Notes

The authors declare no competing financial interest.

■ ACKNOWLEDGMENTS

The National Natural Science Foundation of China (22225104, 22071077, and 92356302) and China Postdoctoral Science Foundation (2022TQ0115 and 2022M711297) are acknowledged for their financial support.

■ REFERENCES

(1) Zhu, Y.; Yang, B.; Chen, S.; Du, J. Polymer Vesicles: Mechanism, Preparation, Application, and Responsive Behavior. *Prog. Polym. Sci.* **2017**, *64*, 1−22.

(2) Zhu, Y.; Wang, F.; Zhang, C.; Du, J. Preparation and Mechanism Insight of Nuclear Envelope-like Polymer Vesicles for Facile Loading of Biomacromolecules and Enhanced Biocatalytic Activity. *ACS Nano* **2014**, *8* (7), 6644−6654.

(3) Meeuwissen, S. A.; Rioz-MartÍnez, A.; de Gonzalo, G.; Fraaije, M. W.; Gotor, V.; van Hest, J. C. M. Cofactor Regeneration in Polymersome Nanoreactors: Enzymatically Catalysed Baeyer−Villiger Reactions. *J. Mater. Chem.* **2011**, *21* (47), 18923−18926.

(4) Gaitzsch, J.; Huang, X.; Voit, B. Engineering Functional Polymer Capsules toward Smart Nanoreactors. *Chem. Rev.* **2016**, *116* (3), 1053−1093.

(5) Chuanoi, S.; Anraku, Y.; Hori, M.; Kishimura, A.; Kataoka, K. Fabrication of Polyion Complex Vesicles with Enhanced Salt and Temperature Resistance and Their Potential Applications as

Enzymatic Nanoreactors. *Biomacromolecules* **2014**, *15* (7), 2389−2397.
(6) Zhang, W. J.; Hong, C. Y.; Pan, C. Y. Polymerization-Induced Self-Assembly of Functionalized Block Copolymer Nanoparticles and Their Application in Drug Delivery. *Macromol. Rapid Commun.* **2019**, *40* (2), No. e1800279.
(7) Tritschler, U.; Pearce, S.; Gwyther, J.; Whittell, G. R.; Manners, I. 50th Anniversary Perspective: Functional Nanoparticles from the Solution Self-Assembly of Block Copolymers. *Macromolecules* **2017**, *50* (9), 3439−3463.
(8) Hayward, R. C.; Pochan, D. J. Tailored Assemblies of Block Copolymers in Solution: It Is All about the Process. *Macromolecules* **2010**, *43* (8), 3577−3584.
(9) D'Agosto, F.; Rieger, J.; Lansalot, M. RAFT-Mediated Polymerization-Induced Self-Assembly. *Angew. Chem., Int. Ed.* **2020**, *59* (22), 8368−8392.
(10) Wang, X.; An, Z. New Insights into RAFT Dispersion Polymerization-Induced Self-Assembly: From Monomer Library, Morphological Control, and Stability to Driving Forces. *Macromol. Rapid Commun.* **2019**, *40* (2), No. e1800325.
(11) Warren, N. J.; Armes, S. P. Polymerization-Induced Self-Assembly of Block Copolymer Nano-Objects via RAFT Aqueous Dispersion Polymerization. *J. Am. Chem. Soc.* **2014**, *136* (29), 10174−10185.
(12) Huang, J.; Guo, Y.; Gu, S.; Han, G.; Duan, W.; Gao, C.; Zhang, W. Multicompartment Block Copolymer Nanoparticles: Recent Advances and Future Perspectives. *Polym. Chem.* **2019**, *10* (25), 3426−3435.
(13) Cornel, E. J.; Jiang, J.; Chen, S.; Du, J. Principles and Characteristics of Polymerization-Induced Self-Assembly with Various Polymerization Techniques. *CCS Chem.* **2021**, *3*, 2104−2125.
(14) Liu, C.; Hong, C.-Y.; Pan, C.-Y. Polymerization Techniques in Polymerization-Induced Self-Assembly (PISA). *Polym. Chem.* **2020**, *11* (22), 3673−3689.
(15) Penfold, N. J. W.; Yeow, J.; Boyer, C.; Armes, S. P. Emerging Trends in Polymerization-Induced Self-Assembly. *ACS Macro. Letters* **2019**, *8* (8), 1029−1054.
(16) Varlas, S.; Foster, J. C.; O'Reilly, R. K. Ring-Opening Metathesis Polymerization-Induced Self-Assembly (ROMPISA). *Chem. Commun.* **2019**, *55* (62), 9066−9071.
(17) Wang, Y.; Han, G.; Duan, W.; Zhang, W. ICAR ATRP in PEG with Low Concentration of Cu(II) Catalyst: A Versatile Method for Synthesis of Block Copolymer Nanoassemblies under Dispersion Polymerization. *Macromol. Rapid Commun.* **2019**, *40* (2), No. e1800140.
(18) Zhou, C.; Wang, J.; Zhou, P.; Wang, G. A Polymerization-Induced Self-Assembly Process for All-Styrenic Nano-Objects Using the Living Anionic Polymerization Mechanism. *Polym. Chem.* **2020**, *11* (15), 2635−2639.
(19) Grazon, C.; Salas-Ambrosio, P.; Ibarboure, E.; Buol, A.; Garanger, E.; Grinstaff, M. W.; Lecommandoux, S.; Bonduelle, C. Aqueous Ring-Opening Polymerization-Induced Self-Assembly (RO-PISA) of N-Carboxyanhydrides. *Angew. Chem., Int. Ed.* **2020**, *59* (2), 622−626.
(20) Grazon, C.; Salas-Ambrosio, P.; Antoine, S.; Ibarboure, E.; Sandre, O.; Clulow, A. J.; Boyd, B. J.; Grinstaff, M. W.; Lecommandoux, S.; Bonduelle, C. Aqueous ROPISA of α-Amino Acid N-Carboxyanhydrides: Polypeptide Block Secondary Structure Controls Nanoparticle Shape Anisotropy. *Polym. Chem.* **2021**, *12* (43), 6242−6251.
(21) Fielding, L. A.; Derry, M. J.; Ladmiral, V.; Rosselgong, J.; Rodrigues, A. M.; Ratcliffe, L. P. D.; Sugihara, S.; Armes, S. P. RAFT Dispersion Polymerization in Non-Polar Solvents: Facile Production of Block Copolymer Spheres, Worms and Vesicles in n-Alkanes. *Chem. Sci.* **2013**, *4* (5), 2081−2087.
(22) Gyorgy, C.; Derry, M. J.; Cornel, E. J.; Armes, S. P. Synthesis of Highly Transparent Diblock Copolymer Vesicles via RAFT Dispersion Polymerization of 2,2,2-Trifluoroethyl Methacrylate in n-Alkanes. *Macromolecules* **2021**, *54* (3), 1159−1169.
(23) Warren, N. J.; Mykhaylyk, O. O.; Ryan, A. J.; Williams, M.; Doussineau, T.; Dugourd, P.; Antoine, R.; Portale, G.; Armes, S. P. Testing the Vesicular Morphology to Destruction: Birth and Death of Diblock Copolymer Vesicles Prepared via Polymerization-Induced Self-Assembly. *J. Am. Chem. Soc.* **2015**, *137* (5), 1929−1937.
(24) Zhang, Y.; Guan, T.; Han, G.; Guo, T.; Zhang, W. Star Block Copolymer Nanoassemblies: Block Sequence is All-Important. *Macromolecules* **2019**, *52* (2), 718−728.
(25) Qu, Y.; Wang, S.; Khan, H.; Gao, C.; Zhou, H.; Zhang, W. One-pot Preparation of BAB Triblock Copolymer Nano-Objects through Bifunctional Macromolecular RAFT Agent Mediated Dispersion Polymerization. *Polym. Chem.* **2016**, *7* (10), 1953−1962.
(26) Zhang, Y.; Han, G.; Cao, M.; Guo, T.; Zhang, W. Influence of Solvophilic Homopolymers on RAFT Polymerization-Induced Self-Assembly. *Macromolecules* **2018**, *51* (11), 4397−4406.
(27) Huo, M.; Li, D.; Song, G.; Zhang, J.; Wu, D.; Wei, Y.; Yuan, J. Semi-Fluorinated Methacrylates: A Class of Versatile Monomers for Polymerization-Induced Self-Assembly. *Macromol. Rapid Commun.* **2018**, *39* (7), No. e1700840.
(28) Zhang, X.; Boissé, S.; Bui, C.; Albouy, P.-A.; Brûlet, A.; Li, M.-H.; Rieger, J.; Charleux, B. Amphiphilic Liquid-Crystal Block Copolymer Nanofibers via RAFT-Mediated Dispersion Polymerization. *Soft Matter* **2012**, *8* (4), 1130−1141.
(29) Mellot, G.; Guigner, J. M.; Bouteiller, L.; Stoffelbach, F.; Rieger, J. Templated PISA: Driving Polymerization-Induced Self-Assembly towards Fibre Morphology. *Angew. Chem., Int. Ed.* **2019**, *58* (10), 3173−3177.
(30) He, X.; Finnegan, J. R.; Hayward, D. W.; MacFarlane, L. R.; Harniman, R. L.; Manners, I. Living Crystallization-Driven Self-Assembly of Polymeric Amphiphiles: Low-Dispersity Fiber-like Micelles from Crystallizable Phosphonium-Capped Polycarbonate Homopolymers. *Macromolecules* **2020**, *53* (23), 10591−10600.
(31) Oliver, A. M.; Gwyther, J.; Boott, C. E.; Davis, S.; Pearce, S.; Manners, I. Scalable Fiber-like Micelles and Block Co-micelles by Polymerization-Induced Crystallization-Driven Self-Assembly. *J. Am. Chem. Soc.* **2018**, *140* (51), 18104−18114.
(32) Robinson, M. E.; Nazemi, A.; Lunn, D. J.; Hayward, D. W.; Boott, C. E.; Hsiao, M. S.; Harniman, R. L.; Davis, S. A.; Whittell, G. R.; Richardson, R. M.; et al. Dimensional Control and Morphological Transformations of Supramolecular Polymeric Nanofibers Based on Cofacially-Stacked Planar Amphiphilic Platinum(II) Complexes. *ACS Nano.* **2017**, *11* (9), 9162−9175.
(33) Albiges, R.; kLEIN, P.; Roi, S.; Stoffelbach, F.; Creton, C.; Bouteiller, L.; Rieger, J. Water-Based Acrylic Coatings Reinforced by PISA-Derived Fibers. *Polym. Chem.* **2017**, *8* (34), 4992−4995.
(34) Dean, J. M.; Verghese, N. E.; Pham, H. Q.; Bates, F. S. Nanostructure Toughened Epoxy Resins. *Macromolecules* **2003**, *36* (25), 9267−9270.
(35) Kim, Y.; Dalhaimer, P.; Christian, D. A.; Discher, D. E. Polymeric Worm Micelles as Nano-Carriers for Drug Delivery. *Nanotechnology* **2005**, *16* (7), S484−S491.
(36) Thompson, K. L.; Mable, C. J.; Cockram, A.; Warren, N. J.; Cunningham, V. J.; Jones, E. R.; Verber, R.; Armes, S. P. Are Block Copolymer Worms More Effective Pickering Emulsifiers than Block Copolymer Spheres? *Soft Matter* **2014**, *10* (43), 8615−8626.
(37) Hartgerink, J. D.; Beniash, E.; Stupp, S. I. Self-Assembly and Mineralization of Peptide-Amphiphile Nanofibers. *Science* **2001**, *294* (5547), 1684−1688.
(38) Song, S.; Liu, X.; Nikbin, E.; Howe, J. Y.; Yu, Q.; Manners, I.; Winnik, M. A. Uniform 1D Micelles and Patchy & Block Comicelles via Scalable, One-Step Crystallization-Driven Block Copolymer Self-Assembly. *J. Am. Chem. Soc.* **2021**, *143* (16), 6266−6280.
(39) Song, S.; Zhou, H.; Manners, I.; Winnik, M. A. Block Copolymer Self-Assembly: Polydisperse Corona-Forming Blocks Leading to Uniform Morphologies. *Chem* **2021**, *7* (10), 2800−2821.
(40) Gilroy, J. B.; Gadt, T.; Whittell, G. R.; Chabanne, L.; Mitchels, J. M.; Richardson, R. M.; Winnik, M. A.; Manners, I. Monodisperse Cylindrical Micelles by Crystallization-Driven Living Self-Assembly. *Nat. Chem.* **2010**, *2* (7), 566−570.

https://doi.org/10.1021/acs.macromol.4c00768
Macromolecules 2024, 57, 7013−7019

(41) Li, X.; Jin, B.; Gao, Y.; Hayward, D. W.; Winnik, M. A.; Luo, Y.; Manners, I. Monodisperse Cylindrical Micelles of Controlled Length with a Liquid-Crystalline Perfluorinated Core by 1D "Self-Seeding". *Angew. Chem., Int. Ed.* **2016**, *55* (38), 11392−11396.
(42) Blanazs, A.; Ryan, A. J.; Armes, S. P. Predictive Phase Diagrams for RAFT Aqueous Dispersion Polymerization: Effect of Block Copolymer Composition, Molecular Weight, and Copolymer Concentration. *Macromolecules* **2012**, *45* (12), 5099−5107.
(43) Byard, S. J.; Williams, M.; McKenzie, B. E.; Blanazs, A.; Armes, S. P. Preparation and Cross-Linking of All-Acrylamide Diblock Copolymer Nano-Objects via Polymerization-Induced Self-Assembly in Aqueous Solution. *Macromolecules* **2017**, *50* (4), 1482−1493.
(44) Bai, Y.; He, J.; Zhang, Y. Ultra-High-Molecular-Weight Polymers Produced by the Immortal Phosphine-Based Catalyst System. *Angew. Chem., Int. Ed.* **2018**, *57* (52), 17230−17234.
(45) Wang, Q.; Zhao, W.; Zhang, S.; He, J.; Zhang, Y.; Chen, E. Y. X. Living Polymerization of Conjugated Polar Alkenes Catalyzed by N-Heterocyclic Olefin-Based Frustrated Lewis Pairs. *ACS Catal.* **2018**, *8* (4), 3571−3578.
(46) Wang, Q.; Zhao, W.; He, J.; Zhang, Y.; Chen, E. Y. X. Living Ring-Opening Polymerization of Lactones by N-Heterocyclic Olefin/$Al(C_6F_5)_3$ Lewis Pairs: Structures of Intermediates, Kinetics, and Mechanism. *Macromolecules* **2017**, *50* (1), 123−136.
(47) Zhao, W.; Wang, Q.; He, J.; Zhang, Y. Chemoselective and Living/Controlled Polymerization of Polar Divinyl Monomers by N-Heterocyclic Olefin Based Classical and Frustrated Lewis Pairs. *Polym. Chem.* **2019**, *10* (31), 4328−4335.
(48) McGraw, M. L.; Clarke, R. W.; Chen, E. Y. Compounded Sequence Control in Polymerization of One-Pot Mixtures of Highly Reactive Acrylates by Differentiating Lewis Pairs. *J. Am. Chem. Soc.* **2020**, *142* (13), 5969−5973.
(49) McGraw, M. L.; Clarke, R. W.; Chen, E. Y. Synchronous Control of Chain Length/Sequence/Topology for Precision Synthesis of Cyclic Block Copolymers from Monomer Mixtures. *J. Am. Chem. Soc.* **2021**, *143* (9), 3318−3322.
(50) Wang, X. J.; Hong, M. Lewis-Pair-Mediated Selective Dimerization and Polymerization of Lignocellulose-Based beta-Angelica Lactone into Biofuel and Acrylic Bioplastic. *Angew. Chem., Int. Ed.* **2020**, *59* (7), 2664−2668.
(51) Zhao, W.; He, J.; Zhang, Y. Lewis Pairs Polymerization of Polar Vinyl Monomers. *Sci. Bull.* **2019**, *64* (24), 1830−1840.
(52) Hong, M.; Chen, J.; Chen, E. Y. Polymerization of Polar Monomers Mediated by Main-Group Lewis Acid-Base Pairs. *Chem. Rev.* **2018**, *118* (20), 10551−10616.
(53) McGraw, M. L.; Chen, E. Y. X. Lewis Pair Polymerization: Perspective on a Ten-Year Journey. *Macromolecules* **2020**, *53* (15), 6102−6122.
(54) Bai, Y.; Wang, H.; He, J.; Zhang, Y. Rapid and Scalable Access to Sequence-Controlled DHDM Multiblock Copolymers by FLP Polymerization. *Angew. Chem., Int. Ed.* **2020**, *59* (28), 11613−11619.
(55) Zhao, W.; Li, F.; Li, C.; He, J.; Zhang, Y.; Chen, C. Lewis Pair Catalyzed Regioselective Polymerization of (E,E)-Alkyl Sorbates for the Synthesis of (AB)n Sequenced Polymers. *Angew. Chem., Int. Ed.* **2021**, *60* (45), 24306−24311.
(56) Wan, Y.; He, J.; Zhang, Y. An Arbitrarily Regulated Monomer Sequence in Multi-Block Copolymer Synthesis by Frustrated Lewis Pairs. *Angew. Chem., Int. Ed.* **2023**, *62* (8), No. e202218248.
(57) Song, Y.; He, J.; Zhang, Y.; Gilsdorf, R. A.; Chen, E. Y.-X. Recyclable Cyclic Bio-based Acrylic Polymer via Pairwise Monomer Enchainment by a Trifunctional Lewis Pair. *Nat. Chem.* **2023**, *15*, 366−376.
(58) Li, C.; Zhao, W.; He, J.; Zhang, Y. Topology Controlled All-(Meth)acrylic Thermoplastic Elastomers by Multi-Functional Lewis Pairs-Mediated Polymerization. *Angew. Chem., Int. Ed.* **2024**, *63*, No. e202401265.
(59) Li, C.; Zhao, W.; He, J.; Zhang, Y.; Zhang, W. Single-Step Expeditious Synthesis of Diblock Copolymers with Different Morphologies by Lewis Pair Polymerization-Induced Self-Assembly. *Angew. Chem., Int. Ed.* **2022**, *61* (24), No. e202202448.
(60) Wang, X.; Hong, M. Precise Control of Molecular Weight and Stereospecificity in Lewis Pair Polymerization of Semifluorinated Methacrylates: Mechanistic Studies and Stereocomplex Formation. *Macromolecules* **2020**, *53* (12), 4659−4669.
(61) Zhang, Z.; Chen, K.; Ameduri, B.; Chen, M. Fluoropolymer Nanoparticles Synthesized via Reversible-Deactivation Radical Polymerizations and Their Applications. *Chem. Rev.* **2023**, *123* (22), 12431−12470.
(62) Zhao, W.; He, J.; Zhang, Y. Research Progress in the Living/Controlled Polymerization of (Meth)acrylate Monomers by Lewis Pair. *Sci. China: Chem.* **2023**, *66* (8), 2256−2266.
(63) Luo, X.; Zhao, S.; Chen, Y.; Zhang, L.; Tan, J. Switching between Thermal Initiation and Photoinitiation Redirects RAFT-Mediated Polymerization-Induced Self-Assembly. *Macromolecules* **2021**, *54* (6), 2948−2959.
(64) Le, D.; Dilger, M.; Pertici, V.; Diabate, S.; Gigmes, D.; Weiss, C.; Delaittre, G. Ultra-Fast Synthesis of Multivalent Radical Nanoparticles by Ring-Opening Metathesis Polymerization-Induced Self-Assembly. *Angew. Chem., Int. Ed.* **2019**, *58* (14), 4725−4731.
(65) Ratcliffe, L. P. D.; McKenzie, B. E.; Le Bouëdec, G. M. D.; Williams, C. N.; Brown, S. L.; Armes, S. P. Polymerization-Induced Self-Assembly of All-Acrylic Diblock Copolymers via RAFT Dispersion Polymerization in Alkanes. *Macromolecules* **2015**, *48* (23), 8594−8607.
(66) Fielding, L. A.; Lane, J. A.; Derry, M. J.; Mykhaylyk, O. O.; Armes, S. P. Thermo-responsive Diblock Copolymer Worm Gels in Non-polar Solvents. *J. Am. Chem. Soc.* **2014**, *136* (15), 5790−5798.
(67) Zhao, W.; Ta, H. T.; Zhang, C.; Whittaker, A. K. Polymerization-Induced Self-Assembly (PISA) - Control over the Morphology of ^{19}F-Containing Polymeric Nano-objects for Cell Uptake and Tracking. *Biomacromolecules* **2017**, *18* (4), 1145−1156.

https://doi.org/10.1021/acs.macromol.4c00768
Macromolecules 2024, 57, 7013−7019